JMEPEG (2020) 29:3253–3263
https://doi.org/10.1007/s11665-020-04809-7


1059-9495/$19.00

# Effect of TiC Content on Tensile Properties, Bend Strength, and Thermal Conductivity of Al-Li-Cu-Mg-Zr Alloy/TiC Composites Produced by Accumulative Roll Bonding

*Aboubakr Medjahed, Bingcheng Li, Ruizhi Wu, Legan Hou, Abdelkhalek Henniche, Abdeldjalil Zegaoui, Mehdi Derradji, and Islam S. Emam*

*(Submitted March 28, 2019; in revised form February 9, 2020; published online April 27, 2020)*

**Composite strips based on an Al-Li-Cu-Mg-Zr alloy reinforced with titanium–carbide (TiC) microparticles were manufactured through the accumulative roll bonding (ARB) process. The microstructure, mechanical and thermal conductivity properties of the processed composites have been experimentally investigated and compared with the as-hot-rolled and un-reinforced states. The microstructure of the reinforced sheets shows the excellent reinforcement's dispersion after the second ARB cycle. In addition, the obtained results indicate that the overall properties of the ARBed strips are enhanced by increasing the TiC content up to 2 wt.%. The processed sheets reinforced with 2 wt.% TiC after two ARB cycles present the superior comprehensive combination of the grain refining, good bonding and proper particle dispersions to reach the outstanding tensile, bending and specific strengths, appropriate tensile elongation and thermal conductivity. Herein, the tensile and bending strengths reach 380.79 and 623.69 MPa, respectively, which are considerably higher than 260.14 and 438.35 MPa, 322.34 and 528.67 MPa of the as-hot-rolled and the un-reinforced sheets after the same cycle, respectively. Moreover, the fracture morphologies of the processed strips exhibit a ductile-shear mixed fracture responding to good elongations of the specimens.**

**Keywords** accumulative roll bonding (ARB), Al-Li-Cu-Mg-Zr alloy, composite strips, mechanical properties, thermal conductivity, titanium-carbide (TiC) microparticles

## 1. Introduction

The aluminum (Al) and their alloys are well-known materials with extensive applications. In recent years, the Al-based metal–matrix composites (MMCs) have attracted expanding consideration in an extensive variety of applications because of their interesting properties, such as superior strength, good wear resistance and high specific modulus (Ref 1-3). Several methods have been used to manufacture the MMCs including powder metallurgy (PM) (Ref 4, 5), spray forming (Ref 6) and squeeze casting (Ref 7, 8). Lu et al. (Ref 9), Alizadeh, and Paydar (Ref 10) successfully used the ARB to manufacture the MMCs. The ARB technique was extensively investigated to manufacture the MMCs reinforced by ceramic particles (Ref 11-14) due to the fast production rate without any necessity of a protective atmosphere and easy to be performed through only a conventional roll milling (Ref 15, 16).

To date, among a wide range of reinforcements, particles are more typical than whiskers, platelets or even fibers due to their low manufacture cost, variety of reinforcements and isotropic properties of the final structures (Ref 2, 14). Many types of MMCs were fabricated via the ARB on various Al alloys using ceramic particles as reinforcements, such as the Al/SiC, Al/$Al_2O_3$, Al/$B_4C$ and Al/WC (Ref 13, 15, 17, 18). Herein, the temperature and reduction are two key factors, which are critical preconditions for an adequate bonding behavior of composite structures. It is found that the cold-ARB method has poor bonding behavior caused by the severe work hardening (Ref 18, 19), though a high thickness reduction insures the good quality of bonding between the composite layers (Ref 20-22).

In the aerospace/aeronautical applications, the Al-Li alloys have been proved to be of a great concern due to their excellent combinations of low density and high stiffness, in which good specific properties are always at a premium (Ref 23-26). With the recent developments in the composite materials, such as fiber–metal laminates (FMLs) and polymer composites (PCs) that provide the combination of high strength and low density (Ref 27-30), it is a commercial interest to use the severe plastic deformation method (SDP), such as the ARB to improve the performances of the Al-Li systems through the grain refinement and ceramic particles reinforcement. In this context, several works investigated the effect of varying the reinforcement's

**Aboubakr Medjahed**, Key Laboratory of Superlight Materials and Surface Technology, Ministry of Education, Harbin Engineering University, Harbin 150001, People's Republic of China; and Laboratoire Génie des Matériaux, École Militaire Polytechnique, BP17 Bordj El-Bahri, 16046 Algiers, Algeria; **Bingcheng Li, Legan Hou, Abdeldjalil Zegaoui, Mehdi Derradji,** and **Islam S. Emam**, Key Laboratory of Superlight Materials and Surface Technology, Ministry of Education, Harbin Engineering University, Harbin 150001, People's Republic of China; **Ruizhi Wu**, Key Laboratory of Superlight Materials and Surface Technology, Ministry of Education, Harbin Engineering University, Harbin 150001, People's Republic of China; and College of Science, Heihe University, Heihe 164300, People's Republic of China; and **Abdelkhalek Henniche**, Laboratoire Génie des Matériaux, École Militaire Polytechnique, BP17 Bordj El-Bahri, 16046 Algiers, Algeria. Contact e-mails: Ruizhiwu2006@yahoo.com and rzwu@hrbeu.edu.cn.

content on the overall properties of the processed composites fabricated by ARB (Ref 31-34). However, few studies have been directed to investigate the impacts of various contents of reinforcing particles on the properties of the composites based on the Al-Li alloys processed by the ARB, and no work has assessed the use of this technique to produce Al-Li strips reinforced by sub-micrometer TiC particles. Presently, among the variety of ceramic particles, the TiC is an outstanding reinforcement with high hardness, high modulus, low density, a high melting point and an appropriate thermodynamic stability (Ref 11, 35). The main objective of this present work is to improve qualitatively and quantitatively the overall performances of a laboratory-designed third-generation Al-Li-Cu-Mg-X alloy through the selection of proper alloying elements and thermomechanical processing, which can be further extended to enhance the formability and the feasibility of fabricating ultrafine grain Al-Li alloy reinforced by different contents of the TiC microparticles using the ARB process for developing advanced engineering composites. The microstructure and mechanical and thermal conductivity properties of the processed composites are investigated.

## 2. Experimental

The Al-1.3Li-3.2Cu-0.35Mg-0.11Zr alloy (in wt.%) and titanium–carbide (TiC) microparticles, with an average size less than 1 μm, were used as raw materials for preparing Al-Li composite strips. Figure 1 shows the image of scanning electron microscopy (SEM) and x-ray diffraction (XRD) pattern of the TiC microparticles. The ingots were obtained through melting and casting under argon atmosphere protection and homogenized at 525 °C for 24 h in order to achieve uniform microstructure and properties. Then, the obtained ingots were annealed at 450 °C for 2 h and followed by hot rolling from 4 mm to 1 mm at the same temperature. Subsequently, the hot-rolled sheets with dimensions of 60 mm × 30 mm × 1 mm were degreased in an acetone bath and subsequently scratch brushed. After the surface preparation, 1, 2 and 3 wt.% TiC microparticles were well dispersed at the surface of the sheets. Then, four sheets were stacked and strongly fastened at both ends by a steel wire. Hereafter, the stacked sheets were heated at 450 °C for 5 min and roll bonded with 50% reduction in order to produce an appropriate bonding between the processed sheets. Later, the bonded specimens were cut into four sheets with approximately similar dimensions of the initial sheets before the first cycle. After that, the above process was repeated up to three cycles without adding the TiC microparticles. The schematic illustration of the ARB process to produce composites up to 64 layers is exposed in Fig. 2. For the comparison purpose, the ARB process was conducted to the studied alloy without reinforcements by following the same process described above. Herein, the interval time between the passes of the ARB is around 5 min, while the final thickness is 1 mm. The ARB process was directed without lubricant utilizing a laboratory rolling mill with a diameter of 500 mm at a roll speed of 600 rpm. The optical microscopy (OM) analysis was employed to observe the microstructure and bonding quality of the RD (rolling direction)–ND (normal direction) of the processed composites, which were prepared by a mechanical polishing and etched with a Keller reagent (2.5 mL $HNO_3$, 1.5 mL HCl, 1 mL HF and 95 mL $H_2O$). The scanning electron microscopy (SEM) equipped with energy-dispersive spectroscopy (EDS) was used to observe the particles' dispersion, interface between layers and fracture surfaces of the studied strips.

The tensile and bending tests were performed at room temperature on a testing machine at a displacement rate of 2 mm/min. Samples for the thermal conductivity measurements were prepared from the ARB-processed sheets in the form of disks with a diameter of 2.7 mm and thickness of 1 mm and then were studied using a hot-disk apparatus operating at room temperature. In order to denote the different samples, abbreviations of ''ARBXY'' were used in this present paper, where the X represents the content of the TiC microparticles added at the initial cycle (0, 1, 2, and 3 wt.%), and the Y accounts for the ARB number of cycles.

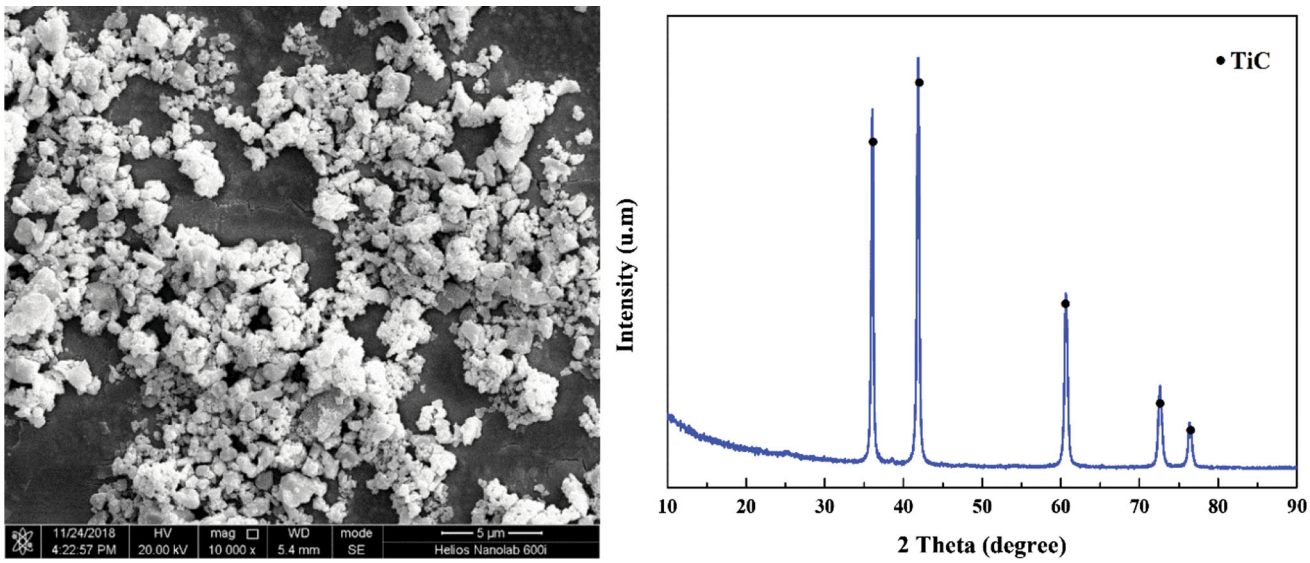


**Fig. 1** Typical SEM image and XRD analysis of the used TiC microparticles

## 3. Results and Discussion

### 3.1 Microstructure

Figure 3 displays the optical micrographs of the prepared specimens with 0, 1, 2 and 3 wt.% TiC at RD-ND plane after two ARB cycles. From this figure, the average grain size decreased after the second cycle to produce ultrafine grains in the outer layers; nevertheless, areas of elongated grains remained in the middle of the samples. This can be clearly observed when a significant decrease in the grain size is detected after the second ARB cycle, and the microstructure consisted of an array of fine grains in the outer layers of the processed strips. In addition, a close examination of the interfaces (Fig. 3), it can be seen from all cases that no delamination detected, when it is a challenging task to recognize the number and interfaces of the layers. This is an indicative of the suitable ARB process accompanied with the

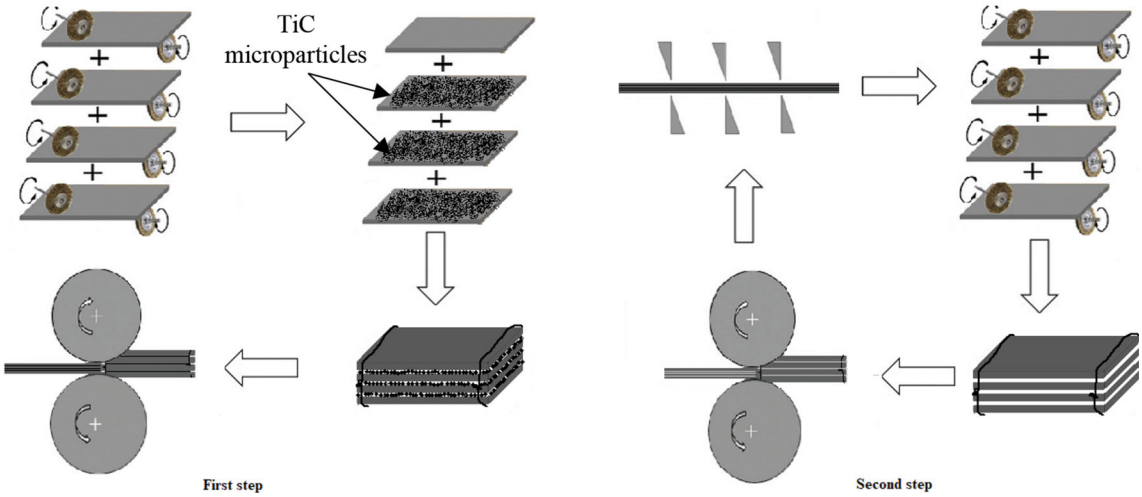


**Fig. 2** Schematic illustration of the ARB process

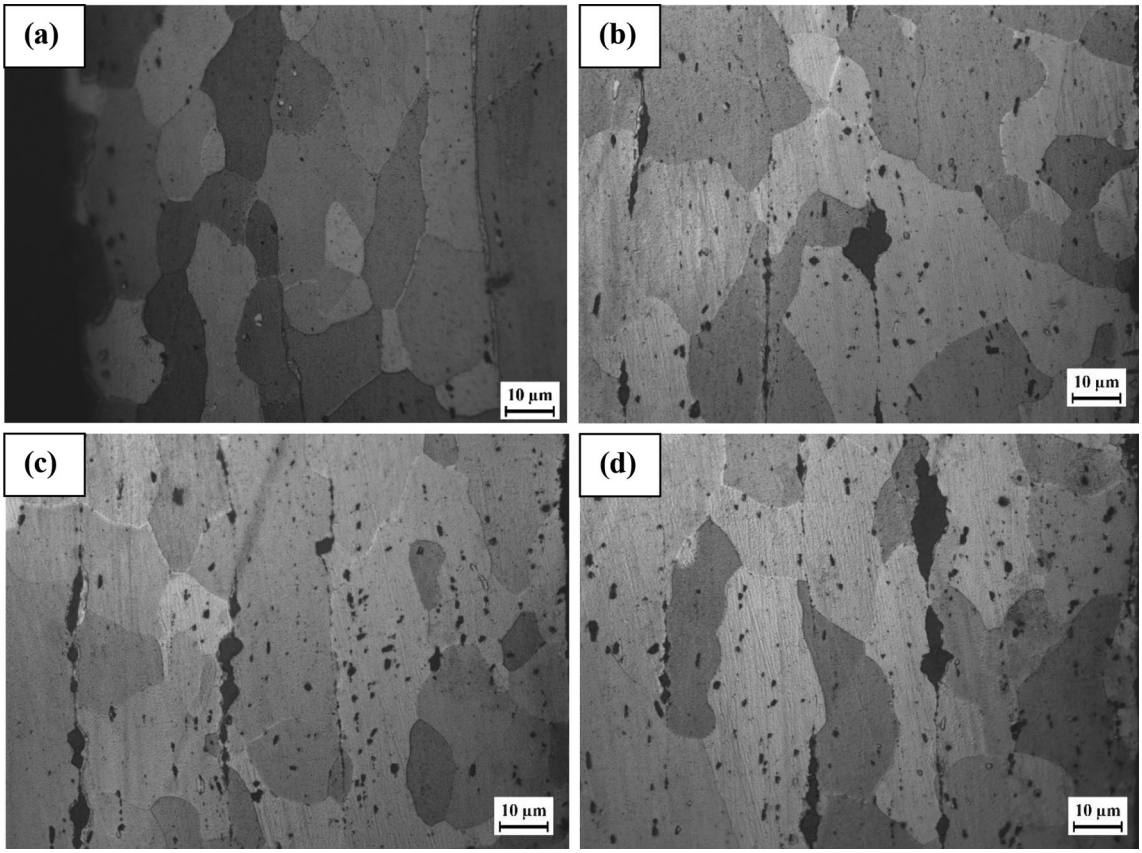


**Fig. 3** Microstructure of the processed composites after two ARB cycles along the RD–ND plane with high magnification: (a) ARB02; (b) ARB12; (c) ARB22 and (d) ARB32 samples

presence of a good bonding at the studied interfaces. Furthermore, the microstructure of the un-reinforced laminates contains fine dispersed grains and the interfaces of layers wholly vanish, as shown in Fig. 3(a). For the reinforced specimens (Fig. 3b, c and d), it can obviously distinct that the amount of the reinforcements represented three amounts (1, 2 and 3 wt.%) within the interfaces of the roll-bonded sheets. Moreover, it is a challenging task to recognize the numbers and interfaces of layers. Thus, all the samples were well prepared with desirable grain refinement in the alloy matrix and good dispersion of the microparticles to improve the overall mechanical properties. In this context, it was reported that the grain refinement during the ARB process of the Al reinforced with ceramic particles is attributed to the hard reinforcement that can be elucidated based on the enriched dislocation density when these particles can produce a rise in the fraction of the high angle boundaries (HABs) in the microstructure. This accelerates the microstructural evolution to obtain a submicron grains structure at a meaningfully lower strain when compared to the un-reinforced alloy (Ref 36, 37). Herein, the evolution of the grain refinement and improvement in the bonding quality after the addition of 1 wt.% TiC was clearly pointed at the interfaces (Fig. 3b), while this content is still almost in low range to reach the peak mechanical properties. Further increase in the content to 2 wt.% (Fig. 3c) presented a combination of an enhanced distribution of the microparticles accompanied with a good bonding behavior within the alloy sheets and grains refining caused by the additional local straining around the embedded microparticles and accompanied by further strengthening that conducted to the enhancement in the overall properties. However, for the reinforced strips with 3 wt.% as displayed in Fig. 3(d), many particles clustering were detected in the studied samples at the bonded interfaces that perhaps produce strict plastic deformation of the grains interiors with high stored energy and further conduct to decline the studied properties. It was stated that the microstructure is influenced by the reinforcement's content. This is strongly linked to the clustering of the ceramic particles when exceeding a certain content of the reinforcements that adversely affects the overall performances (Ref 31-34).

The SEM images along the RD-ND plane are shown in Fig. 4. After the second cycle (16 layers), the bonding behavior is more appropriate with no obvious delamination for the un-reinforced strips (Fig. 4a). For the ARB12 sample (Fig. 4b), fine microparticles are located at the interfaces with a uniform dispersion. After 2 wt.% addition (Fig. 4c), the distribution of the particles turns out to be more uniform accompanied with a detachment of the microparticles from the layer interfaces comparing it with the precedent cycle. Furthermore, the bonding feature between the processed sheets markedly improved. Further rise in the content of the microparticles (Fig. 4d), numerous particles cluster as indicated by arrows. Moreover, Fig. 5 displays a typical SEM image of the developed composites and the corresponding EDS results. The EDS results show that the point A is the TiC particles, while the point B is the Al-Li alloy.

### 3.2 Mechanical Properties and Fracture Morphology

**3.2.1 Tensile Properties.** The tensile stress–strain curves and their corresponding results [Ultimate tensile strength (UTS), uniform elongation (E%)] of the investigated specimens are represented in Fig. 6 and 7, respectively. As for the un-reinforced specimens, after two ARB circles, the ARB02 possesses UTS of 322.3 MPa, while UTS of the hot-rolled specimen (HR) is 260.14 MPa. During the ARB process, it was stated that the strain hardening and grains refinement are two vital mechanisms that have an impact on the strengthening effect (Ref 38, 39). The addition of 1 wt.% TiC shows an enhancement in the UTS for the ARB12 specimen to be around 359.56 MPa associated with the good adhesion and dispersion of the microparticles when compared to the ARB11 sample with a UTS of 308.63 MPa. The processed composite with 2 wt.% addition displays a peak strength value of 379.29 MPa (ARB22), higher than that of the un-reinforced strips and the ARB12 sample, signifying the role of the TiC microparticles in improving the mechanical properties of the prepared composites. This advanced strength is associated with the load transfer from the soft matrix to the hard reinforcements (TiC microparticles) insured by the appropriate bonding after two cycles. In addition, the high strength reinforcement also affects the evolution of the matrix microstructure upon the ARB process and accordingly influences the above-stated strengthening mechanisms (Ref 39, 40) Further increase in the TiC content to 3 wt.% displays a decrease in the UTS for the ARB31, ARB32 and ARB33 samples to achieve the values of about 305.74, 330.38 and 295.45, respectively. This can be explicated by the particle clustering that reduces the quality of the bonding and load transfer between the metal interfaces and the ceramic microparticles. It plastically deforms the grains near the agglomerated regions, as shown in Fig. 3(d).

From Fig. 6 and 7, at the initial stage (first cycle), the composite strips show low elongation values between 14.73 and 16.98% comparing to those of the ARBed sheets after two cycles (ARB02) and the hot-rolled state with elongation values of 17.84 and 23.92%, respectively. The low elongation values can be attributed to the presence of residual porosity accompanied with a minor bonding behavior between the alloy layers and the TiC microparticles. In this context, further increasing the ARB cycles (second cycle) (Fig. 3c), the better-quality interfacial bonding and the enhanced dispersion of the microparticles offer an improvement in the final elongation to rupture for the ARB12 and ARB22 samples to reach the elongations of 19.35 and 20.52, respectively. The reduction in the number of pores caused by the flow of the alloy matrix via the particle clusters enhances the bonding behavior at the interfaces, consequently improving the strength and ductility of the reinforced specimens with 2 wt.% TiC after two ARB cycles (Fig. 6 and 7), though for the ARB32, the presence of some residual microparticles clusters having an important number of voids that are not wholly occupied by the alloy matrix can undesirably affect the elongation of the reinforced sheets (15.83%) comparing it to those of the un-reinforced strips and the reinforced ones with 1 and 2 wt.%. Further, for the reinforced strips after three cycles with 64 layers, the stress concentration results from the occurrence of considerable number of pores within the reinforcements clusters that cause the initiation of micro-cracks. Hence, the tensile strength and the ductility of the processed reinforced specimens deteriorate when compared to the previous cycles with the same reinforcement contents. Besides, the densities of the composites were perceived to increase with increasing the filler loading from 1 to 3 wt.% and the number of the ARB process, as shown in Fig. 8. It seems to display that there is a significant

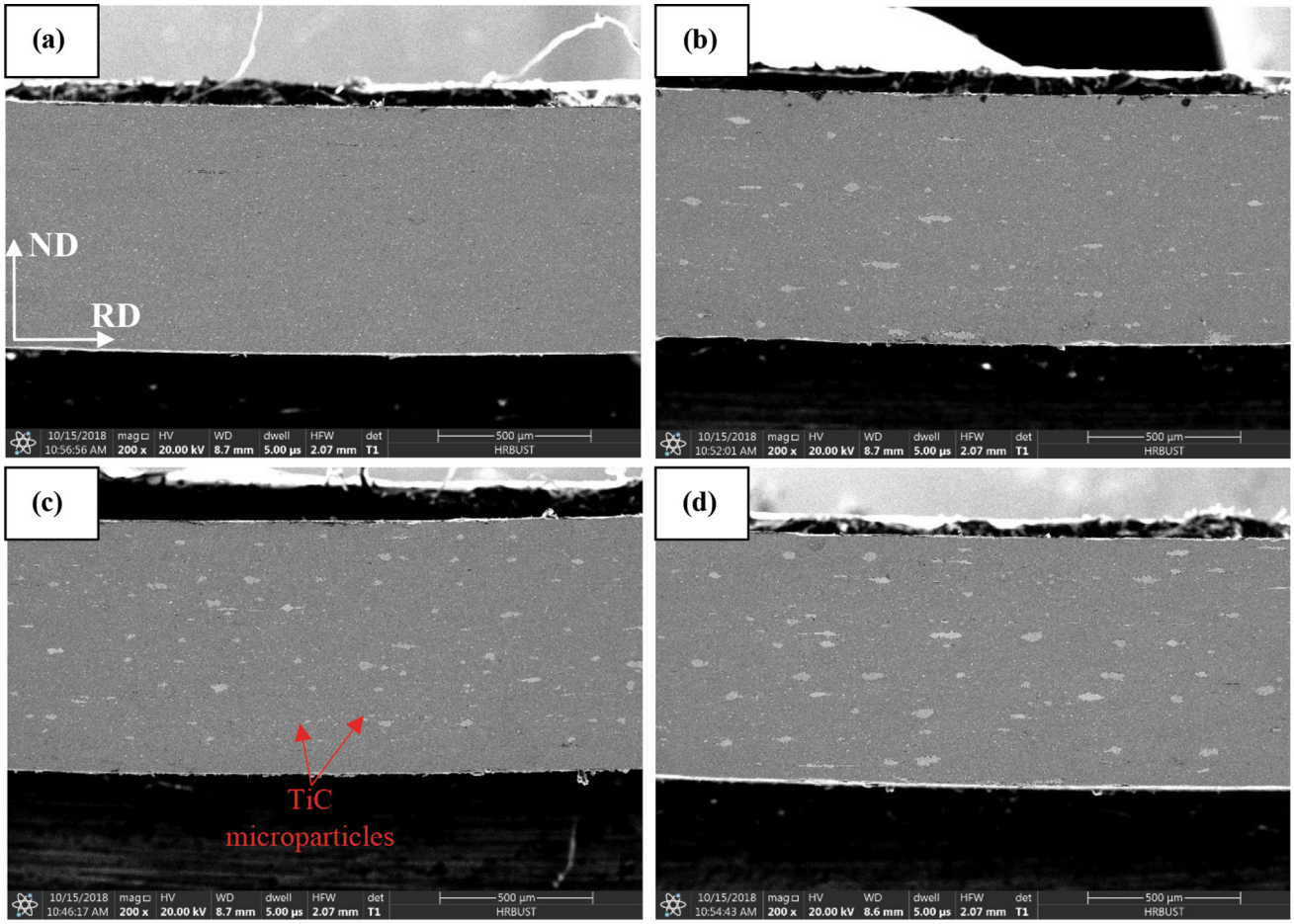


**Fig. 4** SEM images of the studied samples after two ARB cycles along the RD–ND plane: (a) un-reinforced; reinforced with (b) 1 wt.%; (c) 2 wt.% and (d) 3 wt.% TiC microparticles

dissimilarity between the specific tensile strengths of the investigated specimens. Herein, the reinforced strips exhibited great enhancements over the un-reinforced ones even with the relatively higher density resulted from the addition of the microparticles (Fig. 8). Therefore, the reinforced sheets with 2 wt.% of TiC processed by two ARB cycles presented an increment of 30 and 14%, when relatively compared to the as-hot-rolled and un-reinforced sheets at the same cycle, respectively.

Various studies have been carried out in relation to explore of the production and properties of the metal–matrix composite materials. At this point, it seems interesting, to compare the obtained experimental tensile results in this current study with those previously reported regarding the composites fabricated using different techniques such as squeeze casting, powder metallurgy and spray forming. In this context, the mechanical properties of squeeze cast 6061 aluminum alloy and its composite reinforced with SiC particles were investigated (Ref 40). The strength of the composites was significantly higher (200 MPa) than that of the base material (144 MPa). However, the ductility of the processed composites (1.9%) was less than that of the un-reinforced samples (8.9%). Furthermore, in the work of Dhoria et al. composites of Al6351/SiC were produced via squeeze casting using the 6351 aluminum alloy as matrix (Ref 41). They pointed out an increase in the tensile strength for the reinforced composites (166.7 MPa) when compared to the pure alloy (132.5 MPa), while the elongation decreased from 8.12% (pure Al) to 3.26% for the reinforced samples. Additionally, powder metallurgy was used in the fabrication of Al matrix composite reinforced by alumina (Ref 5). As the results indicated, the reinforced samples had improved strength properties (275 MPa) than the pure Al (140 MPa). On the other hand, the final strain decreased from 9% (pure Al) to 5.8% (reinforced samples). As well, some researchers used the spray forming technology to produce Al matrix composites reinforced by basalt particles (BP) (Ref 42). They exhibited the improvement in the ultimate tensile strength of BP/Al matrix reaching 699 MPa, which increase by 10.9% compared with the un-reinforced samples. Undeniably, the former results confirmed that the used processes improved the tensile strength when compared to the un-reinforced materials, while in our current study using the ARB process, the tendency of the enhancement was considerably remarkable between the un-reinforced strips and the reinforced ones particularly after the addition of 2 wt.% TiC. Besides, it was found from our obtained results that the strain to failure of the reinforced strips presented improved performance after the addition of 1 and 2 wt.% TiC when compared to the un-reinforced ones, which is not in the same trend as those previously reported that exhibited generally a decline in the final strain to failure. This explained the ability of the ARB to produce novel composite strips with outstanding properties for the designed Al-Li-Cu-Mg-X alloy.

Figure 9 displays the fracture microstructures of the studied samples. For the un-reinforced sheets, the size and deepness of

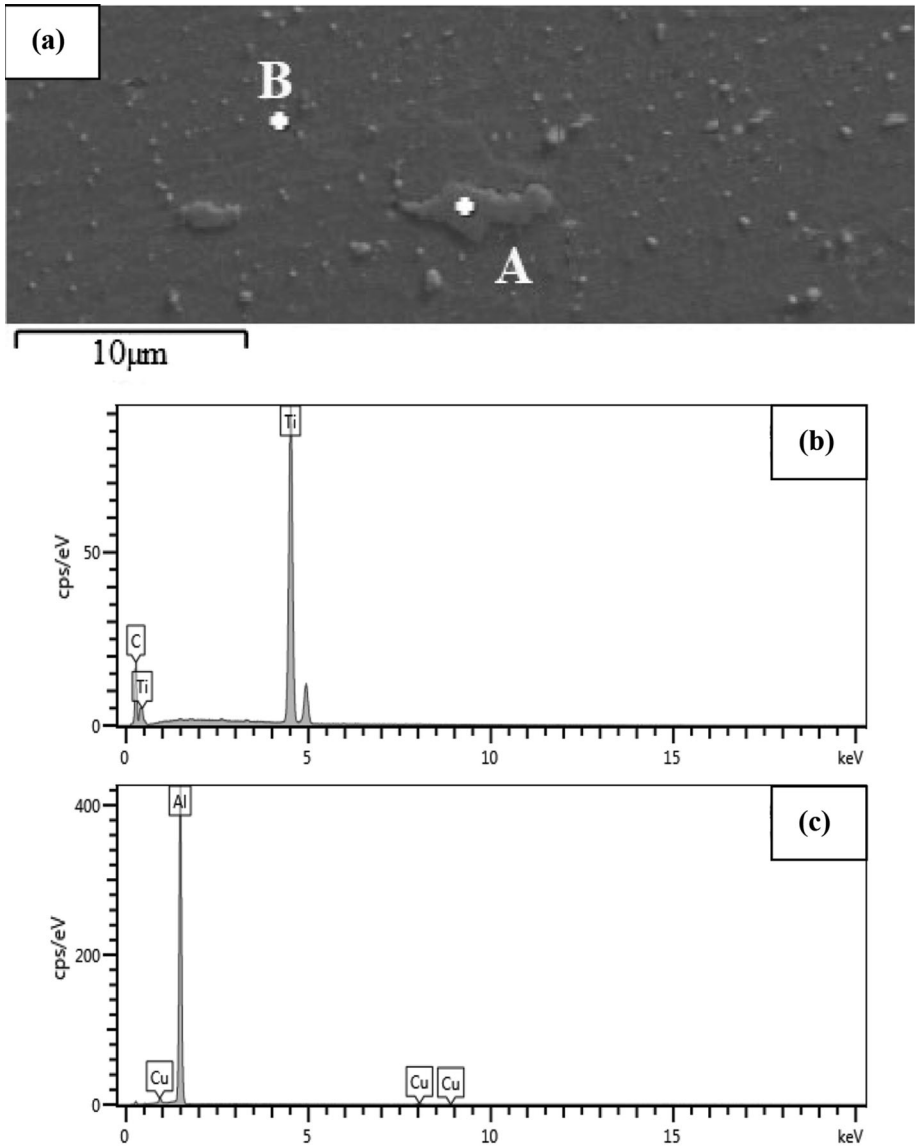


**Fig. 5** (a) Typical SEM image of the processed composites; (b) and (c) EDS results corresponding to points A and B, respectively

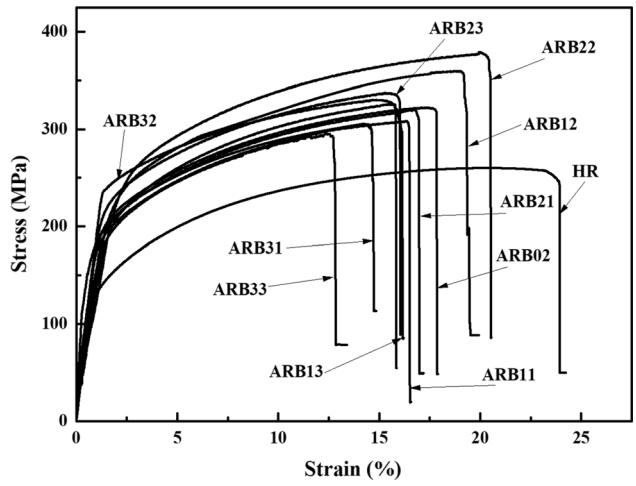


**Fig. 6** Stress–strain curves of the studied strips obtained along the rolling direction

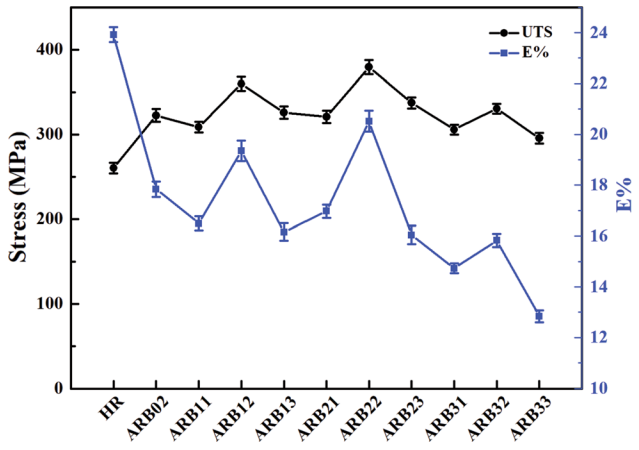


**Fig. 7** Ultimate tensile strengths and elongations of the studied strips obtained along the rolling direction

dimples in the ARBed specimen are smaller that caused the reduction in ductility, which in turn influences the plastic deformation. The reinforced strips exhibited shallow dimples with somewhat smooth surfaces and tearing strips as the characteristics of the typical ductile-shear-mixed type. The reduction in the dimple size is caused by the grain fragmentation of particles as well as the work hardening (Ref 43, 44). According to Fig. 9(a) and (b), the debonding degree between the microparticles and matrix was evidently reduced when the TiC microparticles were entirely encircled by the metal–matrix. This is an indication for the attained enhancement in the elongation to reach 19.35% for the ARB12 specimen when compared to the ARB02 sample (17.84%). After the addition of 2 wt.% (ARB22 sample), as displayed in Fig. 9(c), the elongation of the specimens improved reaching 20.52%, which resulted from the vanished deep holes accompanied with more homogeneous dispersion of the microparticles. At this stage, a proper bonding behavior between the microparticles and alloy matrix reduces the nucleation sites for the crack initiation and imports a further proficient load transfer from the metal–matrix to the reinforcements. These effects play a serious part in the enhancement of the strength and elongation of the processed strips after the second ARB cycle. Moreover, the fracture morphology of the ARB32 sample contains notable microparticles clusters and deep holes caused by the weak bonding, as shown in Fig. 9(d). These holes serve as a key source for the nucleation and propagation of cracks, early appearance of fracture and consequently lower the elongation of the processed composites (15.83%).

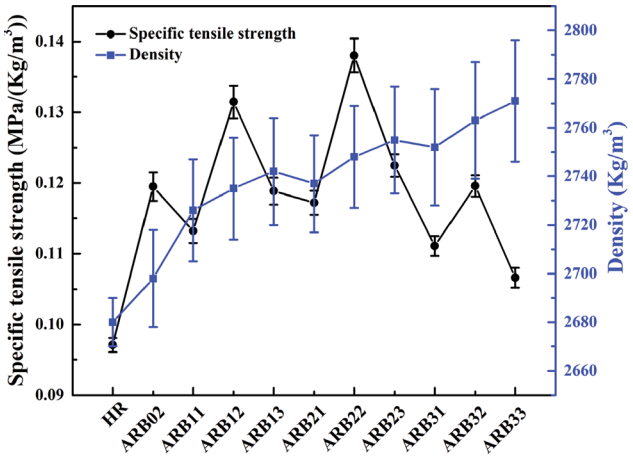


**Fig. 8** Variation in the density and specific tensile strength for the studied specimens

**3.2.2 Bending Properties.** Figure 10 displays the results of the bending tests for the processed strips after diverse ARB cycles. The bending strength (UBS) is improved with the

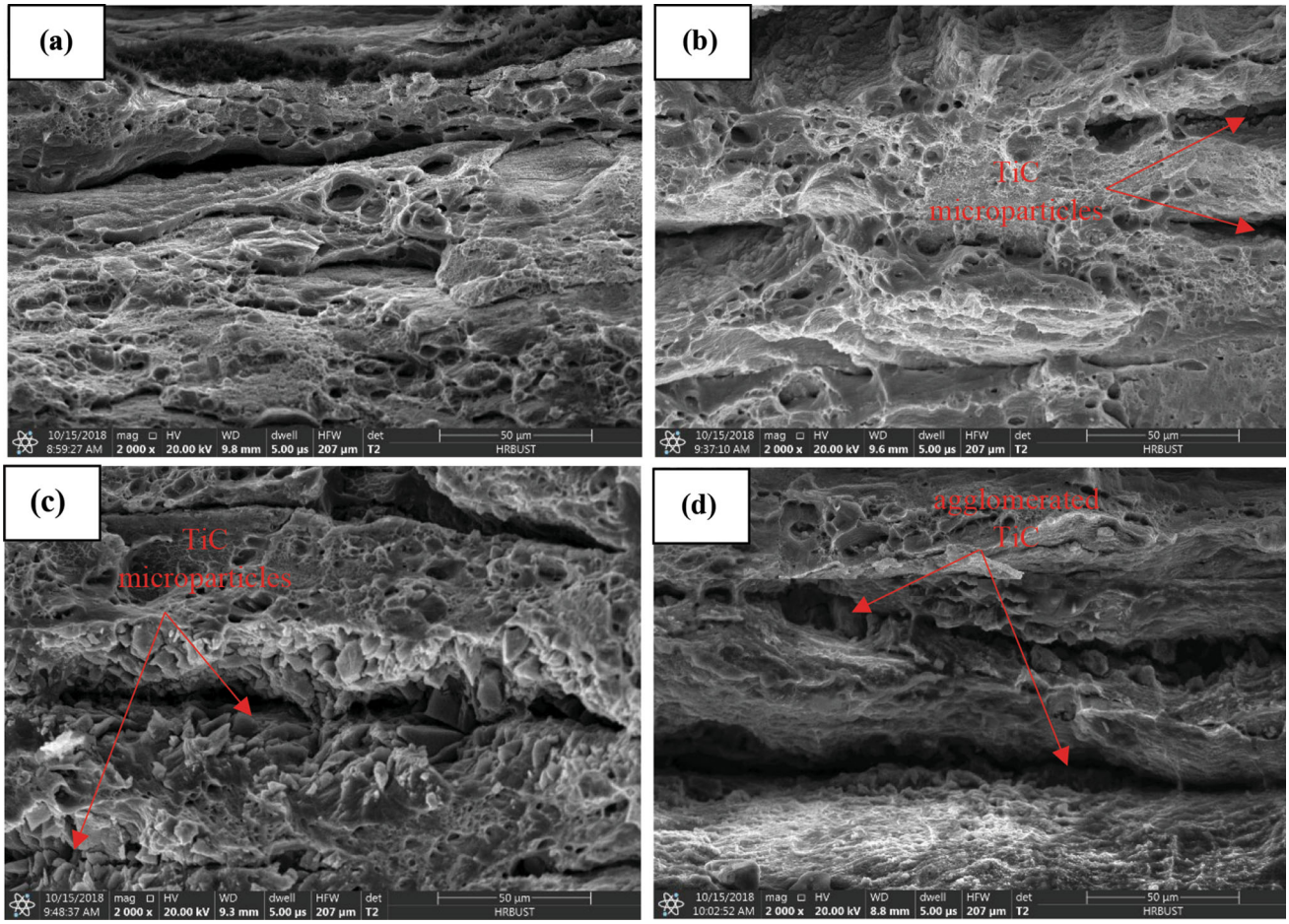


**Fig. 9** Fracture morphology of the processed composite strips after the second cycle for the (a) ARB02; (b) ARB12; (c) ARB22; and (d) ARB32 samples

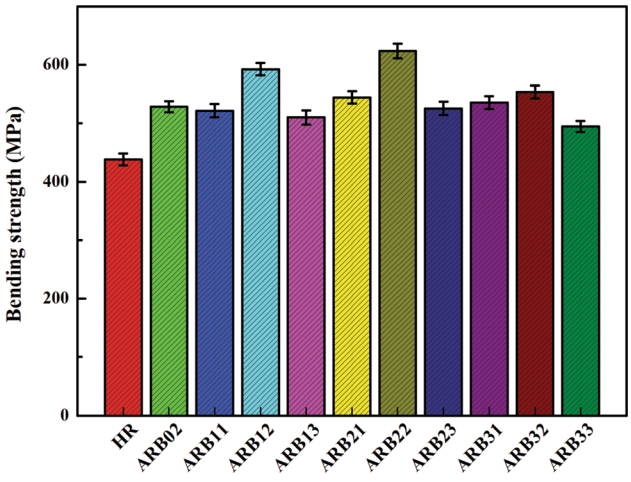


**Fig. 10** Bending strength of the studied specimens

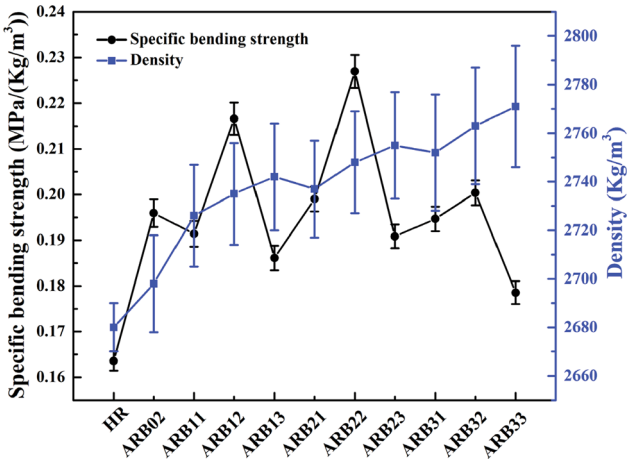


**Fig. 11** Variation in the density and specific bending strength for the studied specimens

increase in the ARB cycle for the un-reinforced sheets. After two cycles (ARB02), the bending strength reaches 528.67 MPa from 438.35 MPa of the hot-rolled specimen. This is can be related to that, after the second cycle, the microstructure displays a better combination of grain refinement, strain hardening and high-quality bonding between the 16 interfaces (Fig. 3a). The bending strength of the reinforced composites (with 1, 2 and 3 wt.% TiC) with different ARB cycles clearly advances and, respectively, presents the impact of the TiC microparticles' addition on the bending properties. After one ARB cycle for the ARB11, ARB21 and ARB31 samples, the bending strengths reach the values of 521.78, 544.63 and 535.72 MPa, respectively. There is an improvement when compared to the hot-rolled state, even though good bonding and dispersion still not reach the optimum state. The enhancement becomes noticeable in the ARB22 sample with the peak bending strength of 623.69 MPa. It can be ascribed to the good bonding behavior, proper amount and dispersion of the reinforcements in the matrix, as revealed in Fig. 3(c) comparing it to the ARB12 sample (592.45 MPa). It was stated that the quality of the bonding behavior and hardness of the reinforcement particles produce a larger strength enhancement for the ARBed composites (Ref 9, 36). However, for the ARB32 sample, the bending strength decreases to the value of 553.59 MPa due to the apparent TiC microparticles clustering, as presented in Fig. 3(d). Furthermore, after the third ARB cycle (ARB13, ARB23, ARB33), the reduction in the bending strength is caused by the notable agglomeration of the TiC particles accompanied by necking and partial delamination of severely deformed sheets (plastically deformed grains). Moreover, the reinforced strips attained not only the highest bending strength, but also the highest specific properties (UBS/ρ), as exhibited in Fig. 11. Herein, the reinforced sheets with 2 wt.% after the second ARB cycle revealed percent increases approximately of 28 and 14% when compared to the as-hot-rolled and un-reinforced sheets, respectively. Therefore, the processed reinforced strips using the ARB process can be considered promising and sustainable composite materials for structural and multifunctional applications.

Figure 12 displays the failure microstructures of the processed composites after the bending test. There is no obvious crack appearing across the layers along the load direction for the un-reinforced layers (Fig. 12a). Figure 12(b), (c) and (d) specifies that there is no necking as well as no occurrence of fractured layers in the reinforced samples. In addition, the bent-reinforced specimens show the proper connection and high bonding behavior. Herein, these interfaces turn out to be hard distinguished while they are clear in the case of the un-reinforced strips, as presented in Fig. 12(a). In this viewpoint, a required bending property can be insured by the comprehensive combination of the grains refinement, strain hardening, high bonding quality and the proper addition of the harder TiC microparticles.

**3.2.3 Thermal Conductivity.** It should be indicated that the TiC microparticles have a low thermal conductivity (17-22 W/mK) (Ref 35, 45), when the as-hot-rolled and ARB02 samples exhibit a high thermal conductivity of 195.03 and 202.26 W/mK, respectively, as shown in Fig. 13. In this context, as was detailed, the dislocations play like nucleation sites for the major strengthening phases (Ref 46, 47). The variation in the microstructure by the formation of precipitates causes the α-Al matrix to be leaner in alloying elements particularly in the Li, which allowed the facile transfer of the thermal flow through it, accordingly, slightly improved the thermal conductivity when compared to the as-hot-rolled state. Moreover, the thermal conductivity is noticeably reduced for the processed composites related to the low thermal conductivity of the TiC microparticles. Thus, the reinforced ARB11, ARB12 and ARB13 samples with 1 wt.% showed a thermal conductivity of 153.47, 178.97 and 185.25 W/mK, respectively. With increasing the ARB cycles, good bonding is attained and the number of the defects and impurities reduces in the strips that extremely improve the movements of the electrons. The composites reinforced by 2 wt.% display the same trend. The obtained values decreased to be around 142.66, 157.04 and 173.14 (W/mK) for the ARB12, ARB22 and ARB32 samples, respectively. With increasing the content of TiC to 3 wt.%, the tendency of increasing the thermal conductivity remains with expanding the number of the ARB cycle, while the thermal conductivity is reduced compared to the same ARB cycle for the reinforced strips with 1 and 2 wt.%. Considering both the mechanical and thermal conductivity properties of the developed reinforced strips, when the content of the TiC microparticles is 2 wt.%, the strips processed by two ARB cycles possessed the better mechanical properties

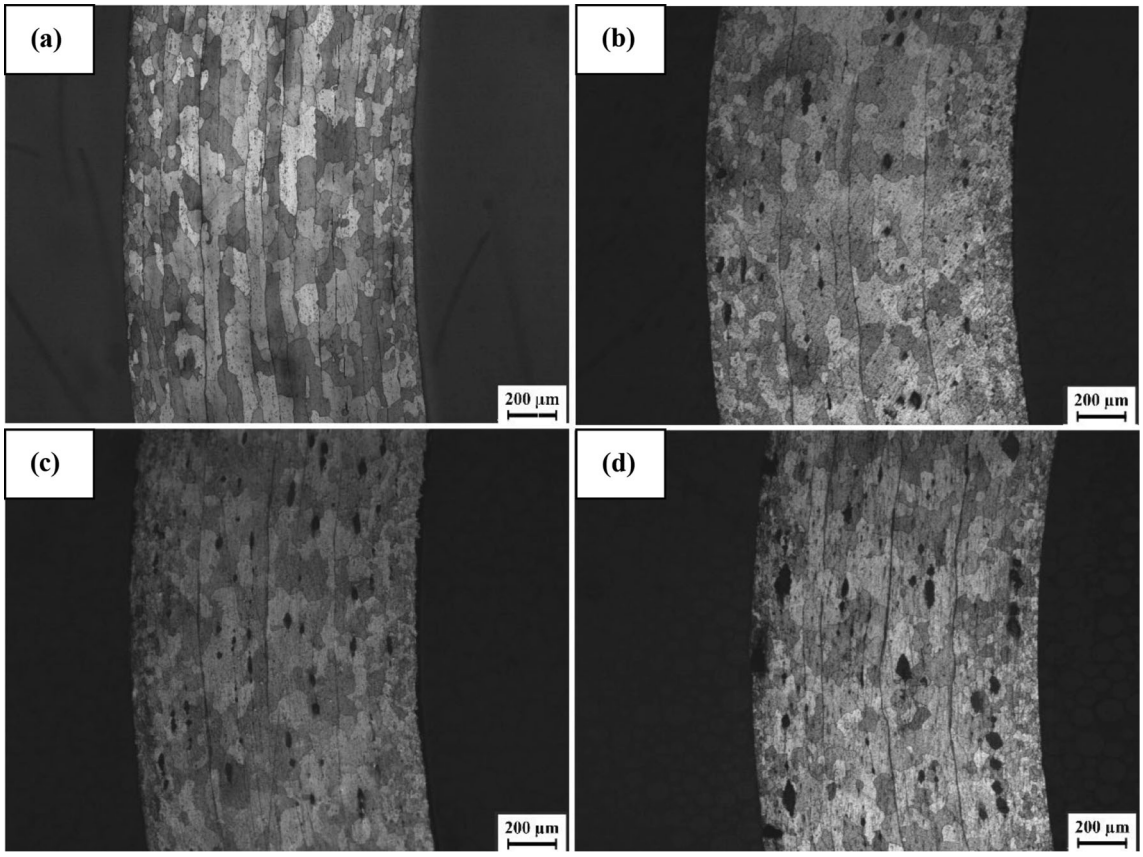


**Fig. 12** Morphology of the studied samples obtained after the bending test after two cycles for the: (a) un-reinforced sheets; (b), (c) and (d) the reinforced ones with 1, 2 and 3 wt.% TiC, respectively

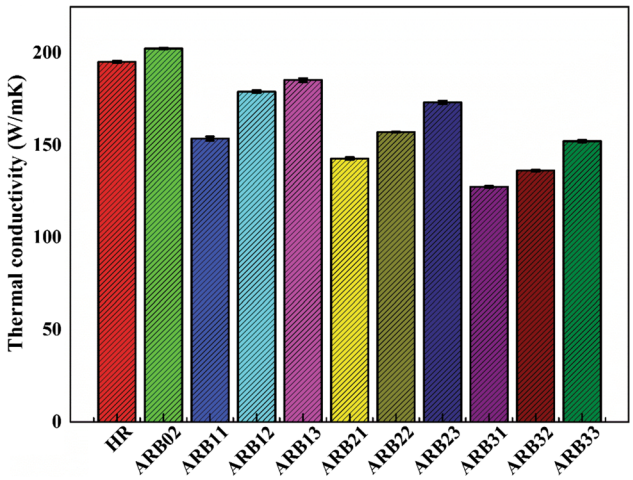


**Fig. 13** Thermal conductivity of the studied strips with different TiC contents

and the appropriate thermal conductivity performances.

Thermal conductivity has been assessed for several materials including metal–matrix composites by means of the following Hasselman–Johnson equation: (Ref 48-50)

$$k_c = k_m \left[ \frac{2k_m + k_p - 2V_f(k_p - k_m)}{2k_m + k_p + V_f(k_m - k_p)} \right]$$

where $k_c$; $k_m$; and $k_p$ are the thermal conductivities of the composite, matrix and particles, respectively, and $V_f$ is the volume fraction of the added particles. A comparison of the measured results of the processed composites after the second ARB cycle with the calculation of the thermal conductivity using the Hasselman–Johnson model is shown in Fig. 14. It displays that the Hasselman–Johnson model affords an adequate agreement to the measured thermal conductivity after the addition of 1 wt.% TiC, while the attained thermal conductivity is still larger than the measured one with increasing the TiC content to 2 and 3 wt.%. Herein, the deviation is most likely due to neglecting the interaction between the matrix and the reinforcements in the proposed model (Ref 48, 50).

## 4. Conclusion

- An excellent dispersion of the added reinforcements (TiC), good bonding behavior, significant strain hardening and grains refining were attained after the second cycle to reach the appropriate properties. Herein, increasing the content of the microparticles to 2 wt.%, the tensile strength enhances to achieve the maximum value of 379.29 MPa, in turn, powerfully advances the bending strength to reach the maximum value of 603.69 MPa. Additionally, the content of the TiC has an improving ef-

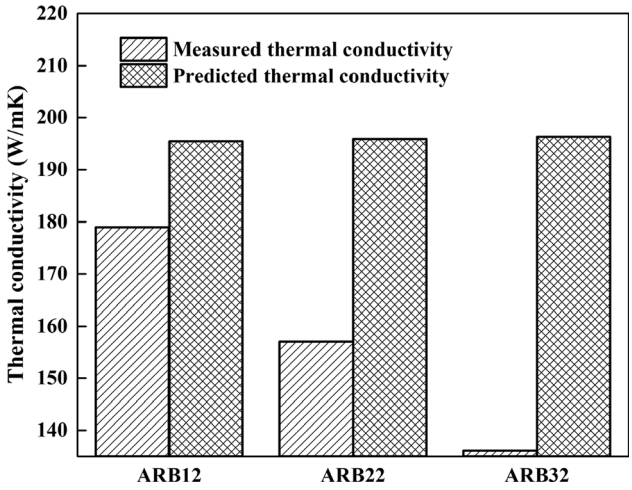


**Fig. 14** Hasselman–Johnson model and the measured thermal conductivity results for the processed composites

fect on the tensile elongation after a certain number of cycles.

- Tensile fractography reveals ductile-shear fracture. The bonding quality of the fracture surface is obviously enhanced for the composites with 1 and 2 wt.% when compared to the un-reinforced sample, while the agglomeration of the microparticles of the reinforced strips with 3 wt.% becomes noticeable.
- The content of the TiC microparticles and the number of the ARB cycles apparently affect the thermal conductivity. The processed sample with 2 wt.% after the second cycle exhibits the best comprehensive combination of the outstanding mechanical properties and the proper thermal conductivity.

## Acknowledgments

This paper was supported by National Natural Science Foundation of China (51671063, 51771060, 51871068), Heilongjiang Province Natural Science Foundation (ZD2017010), the Fundamental Research Funds for the Central Universities (HEUCFG201834), Harbin City Application Technology Research and Development Project (2017RAQXJ032).

## References

1. J. Moradgholi, A. Monshi, K. Farmanesh, M.R. Toroghinejad, and M.R. Loghman-Estarki, Comparison of Microstructure, Toughness, Mechanical Properties and Work Hardening of Titanium/$TiO_2$ and Titanium/SiC Composites Manufactured by Accumulative Roll Bonding (ARB) Process, *Ceram. Int.*, 2017, **43**(10), p 7701–7709
2. E. Ahmadi, M. Ranjkesh, E. Mansoori, M. Fattahi, R.Y. Mojallal, and S. Amirkhanlou, Microstructure and Mechanical Properties of Al/ZrC/TiC Hybrid Nanocomposite Filler Metals of Tungsten Inert Gas Welding Fabricated by Accumulative Roll Bonding, *J. Manuf. Process.*, 2017, **26**, p 173–177
3. W. Zheng, Y.X. Gao, X.P. Wang, H. Lu, L.F. Zeng, and Q.F. Fang, High Strength and Damping Capacity of LLZNO/Al Composites Fabricated by Accumulative Roll Bonding, *Mater. Sci. Eng. A*, 2017, **689**, p 306–312
4. S. Scudino, G. Liu, K.G. Prashanth, B. Bartusch, and K.B. Surreddi, Mechanical Properties of Al-Based Metal Matrix Composites Reinforced with Zr-based Glassy Particles Produced by Powder Metallurgy, *Acta Mater.*, 2009, **57**, p 2029–2039
5. M. Rahimian, N. Parvin, and N. Ehsani, Investigation of Particle Size and Amount of Alumina on Microstructure and Mechanical Properties of Al Matrix Composite Made by Powder Metallurgy, *Mater. Sci. Eng. A*, 2010, **527**(4–5), p 1031–1038
6. D.B. Miracle and S.L. Donaldson, *Composites*, ASM International, Cleveland, 2001
7. K. Sukumaran, K.K. Ravikumar, S.G.K. Pillai, T.P.D. Rajan, M. Ravi, R.M. Pillai, and B.C. Pai, Studies on Squeeze Casting of Al 2124 Alloy and 2124-10% SiCp Metal Matrix Composite, *Mater. Sci. Eng. A*, 2008, **490**(1–2), p 235–241
8. S.-N. Chou, J.-L. Huang, D.-F. Lii, and H.-H. Lu, The Mechanical Properties of $Al_2O_3$/Aluminum Alloy A356 Composite Manufactured by Squeeze Casting, *J. Alloys Compd*, 2006, **419**(1–2), p 98–102
9. C. Lu, K. Tieu, and D. Wexler, Significant Enhancement of Bond Strength in the Accumulative Roll Bonding Process Using Nano-sized $SiO_2$ Particles, *J. Mater. Process. Technol.*, 2009, **209**(10), p 4830–4834
10. M. Alizadeh and M.H. Paydar, Fabrication of Nanostructure Al/$SiC_P$ Composite by Accumulative Roll-Bonding (ARB) Process, *J. Alloys Compd.*, 2010, **492**(1–2), p 231–235
11. J. Nie, F. Wang, Y. Li, Y. Cao, X. Liu, Y. Zhao, and Y. Zhu, Microstructure evolution and Mechanical Properties of Al-$TiB_2$/TiC In Situ Aluminum-Based Composites during Accumulative Roll Bonding (ARB) Process, *Materials*, 2017, **10**(2), p 109–121
12. A. Fathy, D. Ibrahim, O. Elkady, and M. Hassan, Evaluation of Mechanical Properties of 1050-Al Reinforced with SiC Particles via Accumulative Roll Bonding Process, *J. Compos. Mater.*, 2018, **53**(2), p 209–218
13. M. Reihanian, S. Fayezipour, and S.M. Lari Baghal, Nanostructured Al/SiC-Graphite Composites Produced by Accumulative Roll Bonding: Role of Graphite on Microstructure, Wear and Tensile Behavior, *J. Mater. Eng. Perform.*, 2017, **26**(4), p 1908–1919
14. M.R. Morovvati and B. Mollaei-Dariani, The Formability Investigation of CNT-Reinforced Aluminum Nano-composite Sheets Manufactured by Accumulative Roll Bonding, *Int. J. Adv. Manuf. Technol.*, 2018, **95**(9–12), p 3523–3533
15. P. Farhadipour, M. Sedighi, and M. Heydari Vini, Influence of Temperature of Accumulative Roll Bonding on the Mechanical Properties of AA5083–1% $Al_2O_3$ Composite, *Powder Metall. Met. Ceram.*, 2018, **56**(9–10), p 496–503
16. M. Abbasi and S.A. Sajjadi, Manufacturing of Al–$Al_2O_3$–Mg Multilayered Nanocomposites by Accumulative Roll Bonding Process and Study of Its Microstructure, Tensile, and Bending Properties, *J. Compos. Mater.*, 2017, **52**(2), p 147–157
17. M. Naseri, A. Hassani, and M. Tajally, An alternative Method for Manufacturing Al/$B_4C$/SiC Hybrid Composite Strips by Cross Accumulative Roll Bonding (CARB) Process, *Ceram. Int.*, 2015, **41**(10), p 13461–13469
18. C.Y. Liu, Q. Wang, Y.Z. Jia, B. Zhang, R. Jing, M.Z. Ma, Q. Jing, and R.P. Liu, Evaluation of Mechanical Properties of 1060-Al Reinforced with WC Particles via Warm Accumulative Roll Bonding Process, *Mater. Des.*, 2013, **43**, p 367–372
19. P. Farhadipour, M. Sedighi, and M.H. Vini, Using Warm Accumulative Roll Bonding Method to Produce Al-$Al_2O_3$ Metal Matrix Composite, *Proc. Inst. Mech. Eng. Part B J. Eng. Manuf.*, 2017, **231**(5), p 889–896
20. R. Jamaati and M.R. Toroghinejad, Application of ARB Process for Manufacturing High-Strength, Finely Dispersed and Highly Uniform Cu/$Al_2O_3$ Composite, *Mater. Sci. Eng. A*, 2010, **527**(27–28), p 7430–7435
21. M. Rezayat, A. Akbarzadeh, and A. Owhadi, Fabrication of High-Strength Al/SiCp Nanocomposite Sheets by Accumulative Roll Bonding, *Metall. Mater. Trans. A*, 2012, **43**(6), p 2085–2093
22. L. Hou, T. Wang, R. Wu, J. Zhang, M. Zhang, A. Dong, B. Sun, S. Betsofen, and B. Krit, Microstructure and Mechanical Properties of Mg-5Li-1Al Sheets Prepared by Accumulative Roll Bonding, *J. Mater. Sci. Technol.*, 2018, **34**(2), p 317–323
23. A. Medjahed, B. Li, L. Hou, R. Wu, A. Zegaoui, M. Derradji, and H. Benyamina, Evolution of Microstructure, Mechanical Properties, and Thermal Conductivity of an Al-Li-Cu-Mg-Zr Alloy Processed by Accumulative Roll Bonding (ARB), *JOM*, 2019, https://doi.org/10.1007/s11837-019-03646-x

24. T. Yu, B. Li, A. Medjahed, L. Hou, R. Wu, J. Zhang, and J. Sun, Impeding Effect of the $Al_3$(Er, Zr, Li) Particles on Planar Slip and Intergranular Fracture Mechanism of Al-3Li-1Cu-0.1Zr-X Alloys, *Mater. Charact.*, 2019, **147**, p 146–154
25. A. Medjahed, H. Moula, A. Zegaoui, M. Derradji, A. Henniche, R. Wu, L. Hou, J. Zhang, and M. Zhang, Influence of the Rolling Direction on the Microstructure, Mechanical, Anisotropy and Gamma Rays Shielding Properties of an Al-Cu-Li-Mg-X Alloy, *Mater. Sci. Eng. A*, 2018, **732**, p 129–137
26. A. Medjahed, A. Henniche, M. Derradji, T. Yu, Y. Wang, R. Wu, L. Hou, J. Zhang, X. Li, and M. Zhang, Effects of Cu/Mg Ratio on the Microstructure, Mechanical and Corrosion Properties of Al-Li-Cu-Mg-X Alloys, *Mater. Sci. Eng. A*, 2018, **718**, p 241–249
27. A. Zegaoui, M. Derradji, R. Ma, W. Cai, A. Medjahed, W. Liu, A. Qadeer Dayo, and J. Wang, Silane-Modified Carbon Fibers Reinforced Cyanate Ester/Benzoxazine Resin Composites: Morphological, *Mechanical and Thermal Degradation Properties, Vacuum*, 2018, **150**, p 12–23
28. A. Zegaoui, M. Derradji, R.-K. Ma, W.-A. Cai, A. Medjahed, W.-B. Liu, A.Q. Dayo, J. Wang, and G.-X. Wang, Influence of Fiber Volume Fractions on the Performances of Alkali Modified Hemp Fibers Reinforced Cyanate Ester/Benzoxazine Blend Composites, *Mater. Chem. Phys.*, 2018, **213**, p 146–156
29. A. Medjahed, M. Derradji, A. Zegaoui, R. Wu, and B. Li, Mechanical and Gamma Rays Shielding Properties of a Novel Fiber-Metal Laminate Based on a Basalt/Phthalonitrile Composite and an Al-Li Alloy, *Compos. Struct.*, 2019, **210**, p 421–429
30. A. Medjahed, M. Derradji, A. Zegaoui, R. Wu, B. Li, Y. Wang, L. Hou, J. Zhang, and M. Zhang, Fabrication Process, Tensile, and Gamma Rays Shielding Properties of Newly Developed Fiber Metal Laminates Based on an Al-Li Alloy and Carbon FibersTungsten Carbide Nanoparticles Reinforced Phthalonitrile Resin Composite, *Adv. Eng. Mater.*, 2018, **21**(2), p 1800779
31. M. Sedighi, M.H. Vini, and P. Farhadipour, Effect of Alumina Content on the Mechanical Properties of AA5083/$Al_2O_3$ Composites Fabricated by Warm Accumulative Roll Bonding, *Powder Metall. Met. Ceram.*, 2016, **55**(7–8), p 413–418
32. C.Y. Liu, Q. Wang, Y.Z. Jia, B. Zhang, R. Jing, M.Z. Ma, Q. Jing, and R.P. Liu, Effect of W Particles on the Properties of Accumulatively Roll-Bonded Al/W Composites, *Mater. Sci. Eng. A*, 2012, **547**, p 120–124
33. M. Alizadeh, Effects of Temperature and $B_4C$ Content on the Bonding Properties of Roll-Bonded Aluminum Strips, *J. Mater. Sci.*, 2012, **47**(11), p 4689–4695
34. Y.-C. Kang and S.L.-I. Chan, Tensile Properties of Nanometric $Al_2O_3$ Particulate-Reinforced Aluminum Matrix Composites, *Mater. Chem. Phys.*, 2004, **85**(2–3), p 438–443
35. J. Cabrero, F. Audubert, and R. Pailler, Fabrication and Characterization of Sintered TiC–SiC Composites, *J. Eur. Ceram. Soc.*, 2011, **31**(3), p 313–320
36. C.W. Schmidt, C. Knieke, V. Maier, H.W. Höppel, W. Peukert, and M. Göken, Accelerated Grain Refinement during Accumulative Roll Bonding by Nanoparticle Reinforcement, *Scr. Mater.*, 2011, **64**(3), p 245–248
37. H. Akbari Beni, M. Alizadeh, M. Ghaffari, and R. Amini, Investigation of grain refinement in Al/$Al_2O_3$/$B_4C$ nano-composite produced by ARB, *Compos. Part B Eng.*, 2014, **58**, p 438–442
38. R. Jamaati and M.R. Toroghinejad, High-Strength and Highly-Uniform Composite Produced by Anodizing and Accumulative Roll Bonding Processes, *Mater. Des.*, 2010, **31**(10), p 4816–4822
39. S. Khoramkhorshid, M. Alizadeh, A.H. Taghvaei, and S. Scudino, Microstructure and Mechanical Properties of Al-Based Metal Matrix Composites Reinforced with $Al_{84}Gd_6Ni_7Co_3$ Glassy Particles Produced by Accumulative Roll Bonding, *Mater. Des.*, 2016, **90**, p 137–144
40. S.S. Reihani, Processing of Squeeze Cast Al6061–30vol% SiC Composites and Their Characterization, *Mater. Des.*, 2006, **27**(3), p 216–222
41. S.H. Dhoria, V.D. Rao, and K.V. Subbaiah, Mechanical and Wear Behaviour of 6351 Al/Gr/SiC Composites Fabricated by Squeeze Casting, *Mater. Today Proc.*, 2019, **1**(18), p 2107–2113
42. C.H. Fan, O.U. Ling, Z.Y. Hu, J.J. Yang, C.H. Gang, and H.G. Yan, Microstructures and Mechanical Properties of BP/7A04 Al Matrix Composites, *Trans. Nonferr. Met. Soc. China*, 2019, **29**(10), p 2027–2034
43. Z. Wang, K.G. Prashanth, S. Scudino, A.K. Chaubey, D.J. Sordelet, W.W. Zhang, Y.Y. Li, and J. Eckert, Tensile Properties of Al Matrix Composites Reinforced with In Situ Devitrified $Al_{84}Gd_6Ni_7Co_3$ Glassy Particles, *J. Alloys Compd.*, 2014, **586**, p S419–S422
44. S.C. Wang and M.J. Starink, Precipitates and Intermetallic Phases in Precipitation Hardening Al–Cu–Mg–(Li) Based Alloys, *Int. Mater. Rev.*, 2005, **50**(4), p 193–215
45. N.E. Prasad, A. Gokhale, and R. Wanhill, *Aluminum-Lithium Alloys*, Elsevier, Amsterdam, 2014
46. J.-X. Xue, J.-X. Liu, G.-J. Zhang, H.-B. Zhang, T. Liu, X.-S. Zhou, and S.-M. Peng, Improvement in Mechanical/Physical Properties of TiC-Based Ceramics Sintered at 1500 C for Inert Matrix Fuels, *Scr. Mater.*, 2016, **114**, p 5–8
47. A. Medjahed, M. Derradji, A. Zegaoui, R. Wu, and B. Li, Processability and Mechanical Properties of Surface-Modified Glass-Fibres/Phthalonitrile Composite and Al–Li Alloy Fibre-Metal-Laminates, *Mater. Sci. Technol.*, 2019, **35**(6), p 661–668
48. A.K. Dewi, S. Yamaguchi, T. Onitsuka, and M. Uno, Thermal Conductivity Estimation of Fully Ceramic Microencapsulated Pellets with $ZrO_2$ as Simulated Particles, *J. Nucl. Mater.*, 2019, **525**, p 145–151
49. K. Mizuuchi, K. Inoue, Y. Agari, Y. Morisada, M. Sugioka, M. Tanaka, T. Takeuchi, J.I. Tani, M. Kawahara, and Y. Makino, Processing of Diamond Particle Dispersed Aluminum Matrix Composites in Continuous Solid–Liquid Co-existent State by SPS and Their Thermal Properties, *Compos. Part B Eng.*, 2011, **42**(4), p 825–831
50. G. Bai, L. Wang, Y. Zhang, X. Wang, J. Wang, M.J. Kim, and H. Zhang, Tailoring Interface Structure and Enhancing Thermal Conductivity of Cu/Diamond Composites by Alloying Boron to the Cu Matrix, *Mater. Charact.*, 2019, **152**, p 265–275